

Mechanisms of terrestrial organic matter accumulation across the Paleocene-Eocene thermal maximum in the Jiangnan Basin, Central China

Xiaojie Fan^{a,1}, Chunlian Wang^{b,1}, Xiaohua Teng^{c,d,*}, David B. Kemp^e, Yangbo Lu^a, Kai Yan^b, Wei Wei^f, Jingyu Zhang^{g,*}

^a School of Earth Resources, China University of Geosciences, Wuhan 430074, China

^b MNR Key Laboratory of Metallogeny and Mineral Assessment, Institute of Mineral Resources, Chinese Academy of Geological Sciences, Beijing 100037, China

^c Department of Tourism, Resources and Environment, Zaozhuang University, Zaozhuang 277160, China

^d Department of Earth Sciences, Utrecht University, Budapestlaan 17, 3584, CD, Utrecht, the Netherlands

^e State Key Laboratory of Biogeology and Environmental Geology and Hubei Key Laboratory of Critical Zone Evolution, School of Earth Sciences, China University of Geosciences, Wuhan 430074, China

^f State Key Laboratory of Geological Processes and Mineral Resources, School of Earth Sciences, China University of Geosciences, Wuhan 430074, China

^g Centre for Marine Magnetism (CM²), Department of Ocean Science and Engineering, Southern University of Science and Technology, Shenzhen 518055, China

ARTICLE INFO

Editor: Dr. Bing Shen

Keywords:

Organic matter
PETM
Saline Lake
Paleoenvironment
Preservation condition

ABSTRACT

Marine settings provide major carbon sinks for organic carbon, and act as a key reservoir that can sequester excess carbon during times of high CO₂ and global warming. Organic carbon burial in lake sediments also plays an important, but perhaps less appreciated, role in the global carbon cycle. However, the fate of organic carbon burial during times of increasing CO₂ and rapid global warming in lacustrine settings is still unclear. This study investigates organic carbon accumulation and its mechanism during the globally significant Paleocene-Eocene Thermal Maximum (PETM, ~56 Ma) hyperthermal event in the Jiangnan Basin, China, based on organic and element geochemistry data. The PETM is identified in our studied rocks based on their broad age constraints and the presence of a 4.3‰ negative excursion in organic carbon isotope. Our study shows that organic carbon accumulation during the PETM in the Jiangnan Basin might be mainly controlled by preservation conditions and sediment accumulation rates (SAR), which responded to changing hydrology/climate. A hot and humid climate during the PETM could lead to an increase in terrestrial input and SAR, which might dilute the overall organic matter concentration. Also, enhanced rainfall could contribute to the ventilation of the lake water and expedite the oxidation of organic matter, thus, contributing to relatively low organic matter concentration in the Jiangnan Basin. In contrast, an arid and relatively low oxygen environment during the post-PETM interval of our studied section created conditions conducive to the retention of organic matter, resulting in high organic matter content. An examination of other terrestrial PETM records reveals that the poor preservation condition of the organic matter and higher SAR might also have been the primary factors for the low organic matter concentrations in PETM terrestrial sections at other subtropical and mid-latitude locations. Compared to marine settings, terrestrial settings may exhibit lower efficiency in sequestering excess CO₂ from the atmosphere through organic carbon burial during the PETM.

1. Introduction

Organic carbon burial is a key component of Earth's carbon cycle, representing a major long-term sink of CO₂ from the ocean-atmosphere carbon reservoirs (Walker et al., 1981; Laurin et al., 2015). Changes in organic matter accumulation can occur and are mechanistically linked

to major geologic events such as global warming, mass extinction, and oceanic anoxia (Bernier, 2003; Kemp et al., 2022). In the early Paleogene, global temperatures were up to 10 °C warmer than today, creating a 'Hothouse' climate state (Westerhold et al., 2018, 2020). During this period, several hyperthermal events occurred, such as the Paleocene-Eocene Thermal Maximum (PETM), and the Eocene Thermal

* Corresponding authors.

E-mail addresses: tengxiaohua88@163.com (X. Teng), zhangjy6@sustech.edu.cn (J. Zhang).

¹ These authors contributed equally to this work.

Maximum 2 (ETM2) (Zachos et al., 2008; Westerhold et al., 2020). These abrupt warming events were associated with rapid atmospheric increases in CO₂ concentration over a geologically short time intervals (Zachos et al., 2008; Sluijs et al., 2009). As the most well-studied Paleogene global warming events, the PETM is understood to have been associated with the addition of thousands of gigatons of ¹²C-enriched carbon into the ocean-atmosphere system (Dickens et al., 1995; Zeebe et al., 2016), most likely from volcanism and perhaps some surficial reservoirs (e.g., methane hydrates). This large-scale addition of ¹²C-enriched carbon had a significant effect on the global carbon cycle (Zachos et al., 2008; McInerney and Wing, 2011), and is manifested in the sedimentary record as a pronounced negative carbon isotope excursion (CIE) affecting all major biospheric reservoirs of carbon (Kennett and Stott, 1991; McInerney and Wing, 2011). It has been proposed that marine organic matter burial in marine environments, especially in continental margin areas, could have been the major sink

sequestering excess carbon during the PETM (John et al., 2008; Kaya et al., 2022; Papadomanolaki et al., 2022). High nutrient inputs and oceanic anoxia driven by warming would not only increase productivity but also enhance organic matter preservation conditions, together resulting in increased organic carbon burial in marine sediments (Jenkyns, 2010; Raven et al., 2018; Wu et al., 2024).

Organic carbon in lakes is also an important part of the global carbon cycle, especially in the transport of carbon from terrestrial sources to freshwater and marine ecosystems, where it occurs both as dissolved and particulate organic carbon (Mendonça et al., 2017; Drake et al., 2018). Some of the terrestrial carbon delivered to lakes is released to the atmosphere as CO₂, but some is ultimately buried in lake sediments (Ma et al., 2023). To date, however, little is known about organic matter accumulation in lacustrine settings in response to the PETM.

In the Jiangnan Basin, a saline lacustrine basin in China, stratigraphically expanded and well-resolved records of the PETM have been

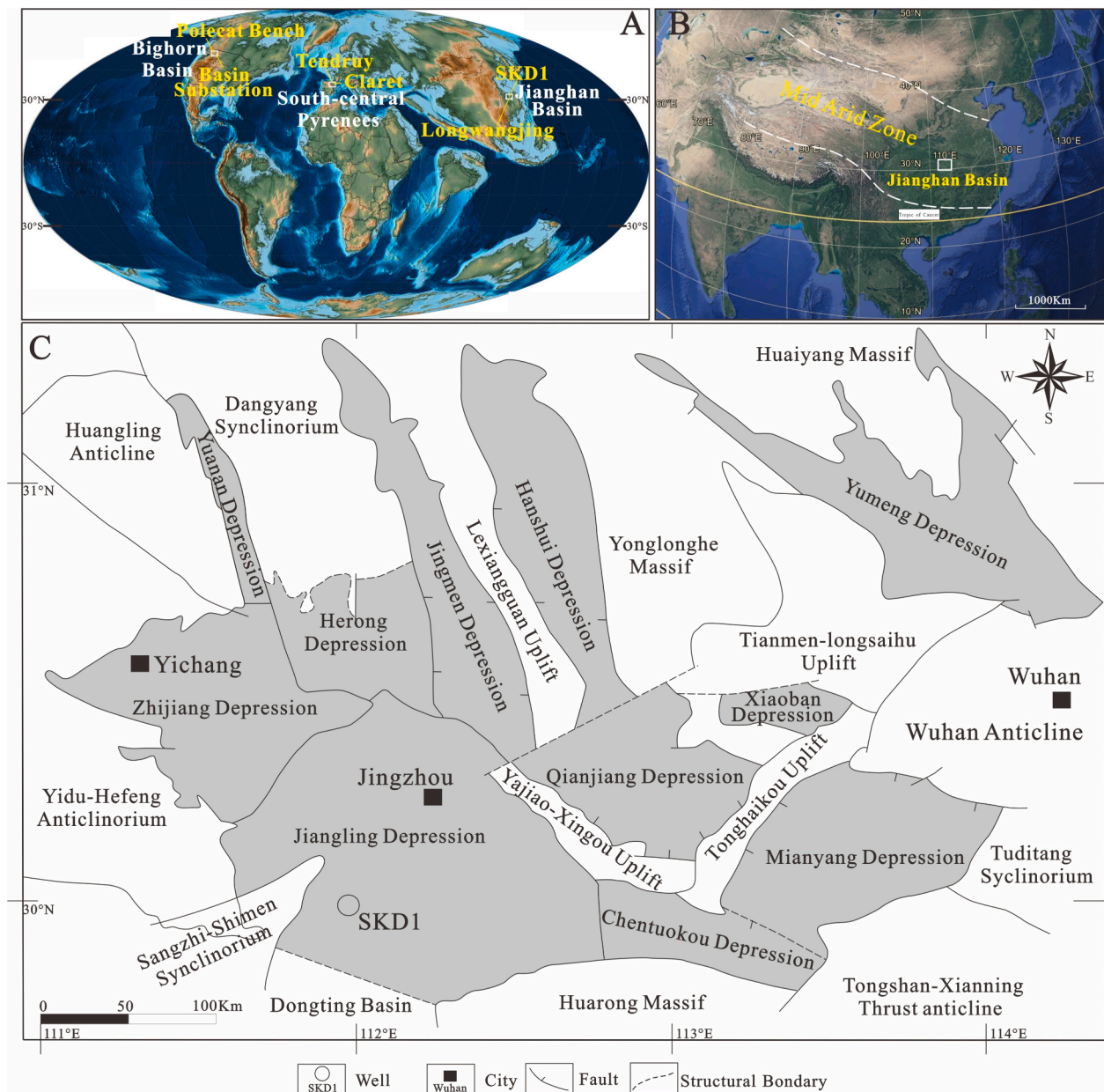


Fig. 1. A. Location of Jiangnan Basin(China), Bighorn Basin(USA), South-central Pyrenees(Spain) on a 55.8 Ma paleographic map (adapted from Scotese, 2014). B. Modern location map of Jiangnan Basin (adapted from Google map), the dotted white line showed mid arid zone modified from (Quan et al., 2014). C. Tectonic divisions of the Jiangnan Basin modified from Yan et al. (2022).

recorded through carbon isotopes and palynological analyses (Teng et al., 2021; Xie et al., 2022; Chen et al., 2023; Luo et al., 2023). As such, it is an ideal site to study terrestrial carbon cycling across the PETM. This study examines a well-preserved PETM record exceeding 60 m in depth retrieved from the SKD1 borehole within the central Jiangnan Basin. Previous researches have accurately delineated the PETM intervals within the SKD1 borehole and have provided comprehensive analyses of petrology, mineralogy, and hydrology (Teng et al., 2019; Teng et al., 2021; Zhang et al., 2024). Building upon prior investigations, this study offers novel insights into the response of organic carbon accumulation in lacustrine environments to the PETM, facilitated by detailed geochemical analyses.

2. Geological setting

The Jiangnan Basin is a Mesozoic–Cenozoic petroliferous rift basin located in Hubei Province, central China, and consists of eleven depressions and four uplifts (Fig. 1B and C) (Philp et al., 1989; Huang and Hinnov, 2014). During the Mesozoic, the subducting Pacific plate triggered the intracontinental orogeny that formed the present tectonic configuration (Schellart and Lister, 2005; Hu et al., 2006). From the Late Cretaceous to the Paleogene, Jiangnan Basin experienced three stages of structural evolution, and deposited a thick succession of sediments (Wu et al., 2017). In the central Jiangnan Basin, the Paleocene to Eocene sedimentary sequence from bottom to top comprises the Shashi, Xingouzui (XGZ), Jingsha, and Qianjiang formations (Huang and Hinnov, 2014). Meanwhile, in the western Jiangnan Basin, the Paleogene sedimentary sequence can be divided into the Gongjiachong, Yangxi, Cheyanghe, and Pailoukou formations (Fig. 2). These strata form a valuable archive of continental paleoclimatic information and also

hydrocarbon-rich.

The SKD1 borehole, situated in the Jiangling Depression (Fig. 1C), preserves a stratigraphically expanded record of the Paleocene Shashi Formation and the Eocene XGZ Formation. The absolute age of the bottom of the XGZ Formation has been constrained to 56 Ma by K–Ar age and cyclostratigraphy (Xu et al., 1995; Huang and Hinnov, 2019). Additionally, the recalibrated paleomagnetic data suggest that the Yangxi Formation was deposited at the same time (56 Ma) (Kong et al., 2024) (Fig. 2). Noteworthy recent investigations have discerned compelling evidence of the PETM within both the XGZ and Yangxi formations (e.g., Teng et al., 2021; Xie et al., 2022; Chen et al., 2023; Luo et al., 2023, and Zhang et al., 2024). Teng et al. (2021) identified the PETM at 1313.6 m to 1376.5 m in the XGZ Formation of the SKD1 borehole, marked by an –10.7‰ magnitude CIE in lacustrine carbonates carbon isotope.

The strata containing the PETM can be divided into three intervals: pre-PETM (1420–1376.5 m), PETM (1376.5–1313.6 m), and post-PETM (1313.6–1250 m). The pre-PETM interval mainly comprises gypsiferous mudstones and argillaceous anhydrite rock (Fig. 3A and B). The PETM interval consists of brownish-red homogeneous mudstones and thin layers of cross-bedding siltstones and sandstones (Fig. 3C and D), and the post-PETM interval contains alternating evaporites (anhydrite, glauberite, and halite) and dolomitic mudstones (Fig. 3E and F) (Teng et al., 2021).

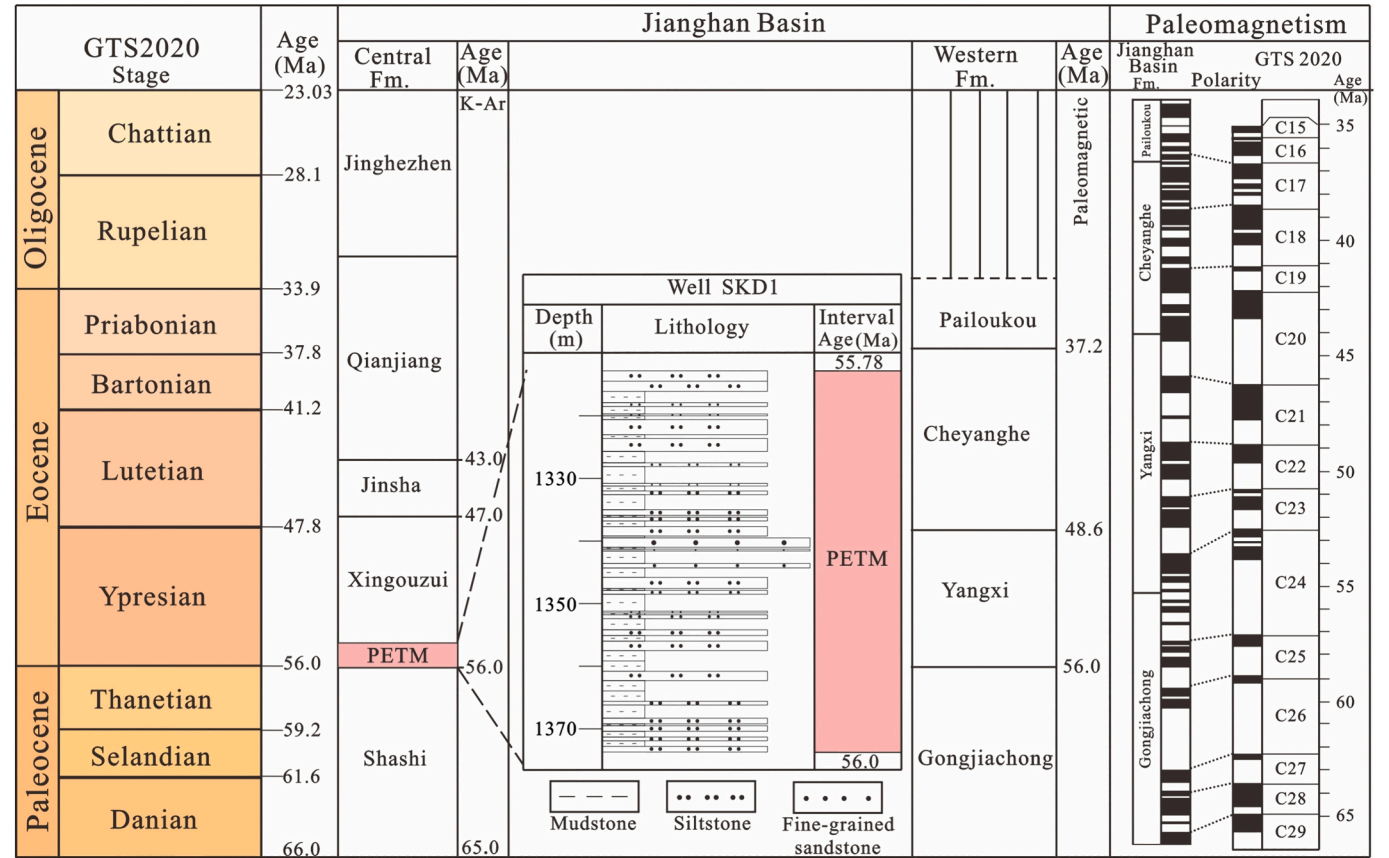


Fig. 2. Comprehensive stratigraphic diagram of the Jiangnan Basin, modified after Xie et al. (2022), with age of central Jiangnan Basin based on (Xu et al., 1995) and PETM age of the SKD1 borehole based on (Zhang et al., 2024). Stratigraphy and paleomagnetic polarity column of the western Jiangnan Basin are from Zhang et al., (1993), and Kong et al. (2024) have recalibrated the paleomagnetic data to GTS2020 (Gradstein et al., 2020).

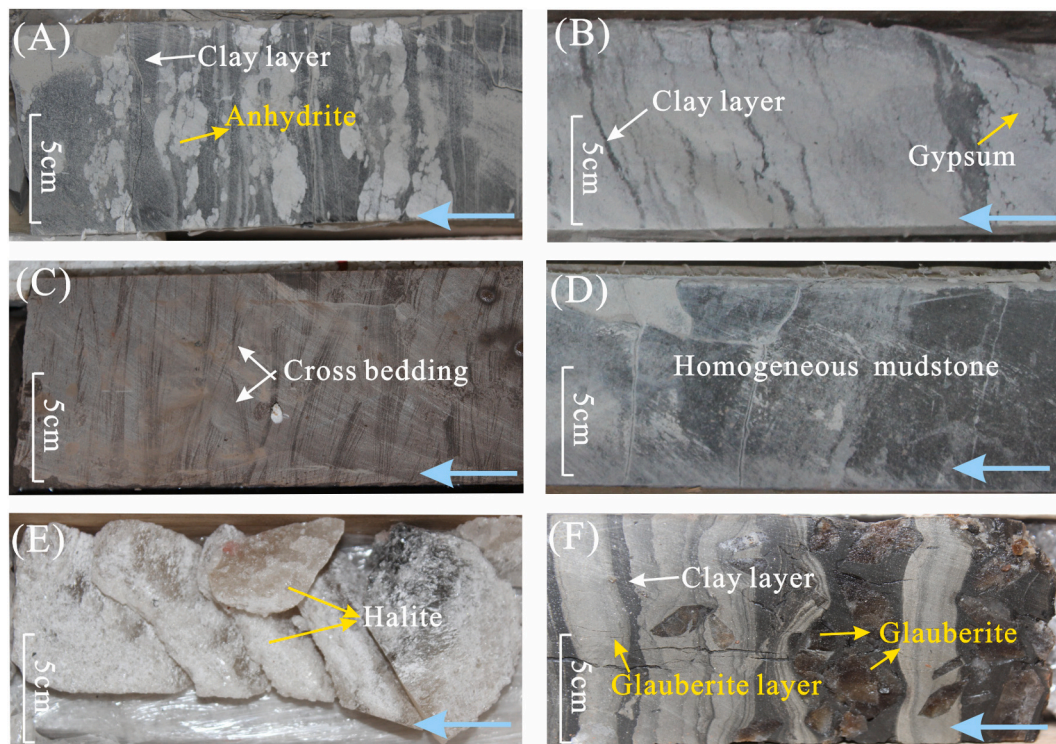


Fig. 3. Photographs of cores show major sedimentary structures in the SKD1 borehole, blue arrow is way-up. A: Gray-green gypsiferous mudstone with well-developed horizontal bedding, and anhydrite is distributed in lumps along the bedding (yellow and white arrow), 1387.3–1387.5 m. B: Gray-white argillaceous anhydrite rock with thin gray-green mudstone layers and gypsum (white and yellow arrow), 1383.3–1383.5 m. C: Siltstone with cross-bedding, 1340.7–1340.9 m. D: Mudstone with massive structure, 1325.1–1325.3 m. E: Thick bedded halite, 1261.7–1261.8 m. F: Light gray gypsiferous dolomite and glauberite layer intercalated with dark gray colored clay layer (white arrow) and glauberite-bearing mudstone (yellow arrow). Yellow arrows show phenocryst-like glauberite crystals (size of 0.5–2 cm), 1252.6–1252.7 m. (For interpretation of the references to colour in this figure legend, the reader is referred to the web version of this article.)

3. Methods

3.1. Total organic carbon (TOC) and organic carbon stable isotope analyses

For total organic carbon (TOC) and organic matter stable isotope ($\delta^{13}\text{C}_{\text{TOC}}$) analyses, 132 samples spanning 1250 m to 1420 m depth were collected from SKD1 borehole and analyzed at the Chinese Academy of Geological Sciences Key Laboratory of Metallogeny and Mineral Assessment. Carbonate was removed from samples with 2 mol/L HCl, then washed with distilled water until the solution was neutral. Dried samples were weighed into tin capsules and tested by an elemental analyzer coupled to a Finnigan MAT-253 mass spectrometer. $\delta^{13}\text{C}_{\text{TOC}}$ was reported relative to the international Vienna Pee Dee Belemnite (VPDB) standard, and the TOC was reported in weight percent organic carbon relative to the mass of the unacidified sample. The relative standard deviations for $\delta^{13}\text{C}_{\text{TOC}}$ and TOC were determined from replicate analyses and were <0.2‰ and 0.1%, respectively.

3.2. Major and trace elements

For the major and trace elements, 43 samples spanning 1250 m to 1420 m depth were collected from SKD1 borehole. Major elements were analyzed by a Philips PW2404 X-ray fluorescence spectrometer. Sample powders were mixed with flux ($\text{Li}_2\text{B}_4\text{O}_7$) at a ratio of 1:8, and then the melting process was carried out at a temperature of 1050 °C for 15 min. The relative standard deviations were below 2%. Trace elements were analyzed by a Jena PQMS Elite inductively coupled plasma-mass spectrometer (ICP-MS). Sample powders were first mixed with 1 mL of HNO_3 and HF. When completely dry, add HNO_3 again and heat to 130 °C for over 12 h. After adding the distilled water, the final solution was

transferred and diluted to 100 g by adding 2% HNO_3 . The relative standard deviations were determined from replicate analyses and were <10%. The experiments were carried out at the Chinese Academy of Geological Sciences Key Laboratory of Metallogeny and Mineral Assessment.

3.3. Proxy calculations

To eliminate terrigenous dilution effects and establish element concentrations relative to reference standard, enrichment factors (X_{EF}) were used to assess the authigenic fraction enrichment of an element in sediments. Here, we use the Al-normalized enrichment factors, calculated by:

$$X_{\text{EF}} = (X/\text{Al})_{\text{sample}} / (X/\text{Al})_{\text{PAAS}} \quad (1)$$

where PAAS is the element concentration in post-Archean average shale (Tribouillard et al., 2006; McLennan, 2001).

A variety of geochemical indicators for instance: rubidium/strontium (Rb/Sr), magnesium/calcium (Mg/Ca), strontium/barium (Sr/Ba), nickel/aluminum (Ni/Al), phosphorus/aluminum (P/Al), and enrichment factors of molybdenum and uranium (Mo_{EF} , U_{EF}), were used to reconstruct paleoenvironment, for detailed principles and applicability, refer to (Dasch, 1969; Tribouillard et al., 1994; Algeo and Maynard, 2004; Tribouillard et al., 2006; Pyle et al., 2017).

4. Results

4.1. Total organic carbon and organic matter stable isotope

TOC content in the study interval ranges from 0.1% to 6.9% (Fig. 4d), and varies in different intervals. The pre-PETM samples have the

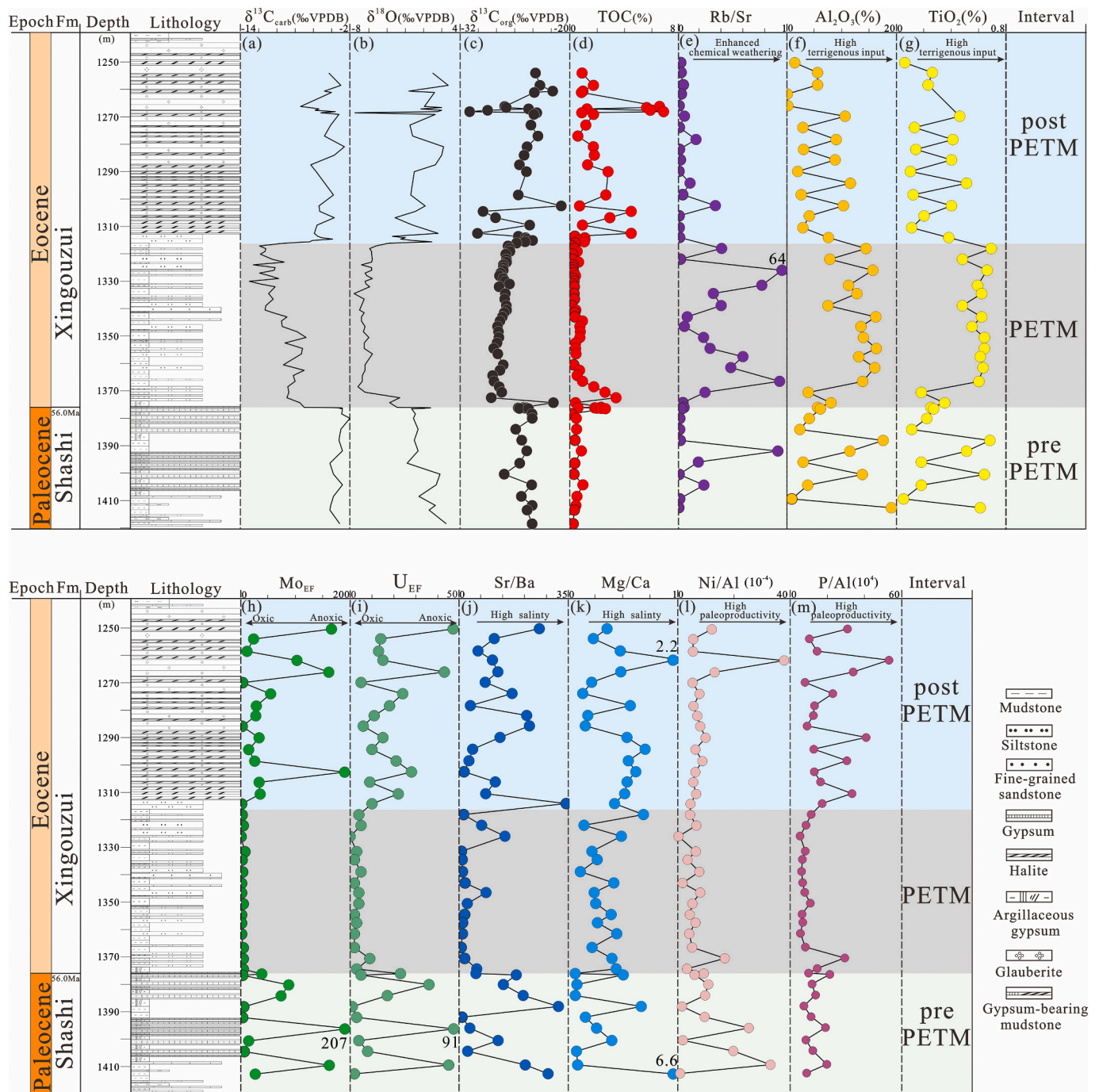


Fig. 4. Stratigraphic profiles of various proxies indicating changes in paleoenvironment through SKD1 borehole across the PETM, $\delta^{13}C_{carb}$ and $\delta^{18}O$ data from Teng et al. (2021).

moderate TOC content (ranging between 0.1% and 2.7%, with an average of 1.4%). The PETM interval has the lowest TOC content, ranging from 0.1% to 3.4%, with an average of 0.5%. Samples from the post-PETM interval have the highest TOC (ranging from 0.4% to 6.9%, with an average of 2.3%).

In the study interval, the minimum $\delta^{13}C_{TOC}$ value is -31.0‰ while the maximum value is -20.9‰ . $\delta^{13}C_{TOC}$ values are stable in the pre-PETM with an average of -25.1‰ and begin to decrease at 1376 m, followed by a slight positive shift at 1374 m (Fig. 4c). Above this, $\delta^{13}C_{TOC}$ drops to -28.6‰ and stabilizes upwards through the PETM. The overall magnitude of the CIE is around 4.3‰, which is calculated by subtracting the most positive immediately prior to the negative $\delta^{13}C_{TOC}$

shift (-24.1‰) at 1374.3 m from the most negative $\delta^{13}C_{TOC}$ value (-28.4‰) at the base of the CIE. Unlike the carbonate carbon isotope ($\delta^{13}C_{carb}$) record, $\delta^{13}C_{TOC}$ values fluctuate in the post-PETM interval, and three negative spikes are observed at 1312.5 m (-30.1‰), 1304–1307 m (-28.8‰), and 1266–1268 m (-27.7‰). Detailed TOC and $\delta^{13}C_{TOC}$ data can be seen in the Supplementary material.

4.2. Major and trace elements

Multiple geochemical indicators were used to reconstruct the paleoenvironment of the SKD1 borehole. SiO_2 is the dominant component with an average of 29.98%, followed by CaO with an average of 16.16%.

Al₂O₃ (Avg. 8.36%), MgO (avg. 5.79%), Na₂O (avg. 5.00%), Fe₂O₃ (avg. 3.34%), and K₂O (avg. 2.13%) all have average concentrations <10%. TiO₂ (avg. 0.39%) and P₂O₅ (avg. 0.11%) have averages concentrations <1%. The most abundant trace element is Sr (avg. 2123 ppm), followed by Mn (avg. 1093 ppm), Ba (avg. 271 ppm), As (avg. 170 ppm), and Li (avg. 121 ppm). Other measured elements have mean concentrations of <100 ppm.

Al₂O₃ and TiO₂ show similar trends, and both elements fluctuate in the pre-PETM interval and have relatively higher values in the PETM (averages of 11.85% and 0.54%, respectively) (Table 1 and Fig. 4f and g). Concentrations then decrease in the post-PETM interval. Rb/Sr ratio is relatively low in the pre- and post-PETM intervals, with an overall mean of <0.05, and is relatively higher in the PETM. Within the PETM, two peaks in Rb/Sr occur at 1326 m and 1366.5 m (Fig. 4e). Sr/Ba and Mg/Ca ratios have high mean values in the pre- and post-PETM intervals, and are much lower in the PETM (Fig. 4 j and k). Both Ni/Al (10⁻⁴) and P/Al (10⁻⁴) exhibit relatively low values in the PETM, with an average of 5 and 9.53 respectively, and are higher in the pre-PETM and post-PETM interval (Fig. 4l and m). Both U_{EF} and Mo_{EF} have an average of 5 in the PETM, and are relatively higher in the pre- and post-PETM intervals (Fig. 4h and i).

5. Discussion

5.1. Reconstruction of the paleohydrology and paleoenvironment

The rapid increase in atmospheric CO₂ concentrations led to global warming during the PETM (Tripathi and Elderfield, 2005). This global warming profoundly altered both global and regional hydrological cycles (Pierrehumbert, 2002; Jones et al., 2018). In the early Paleogene, the subtropical high-pressure zone of the Northern Hemisphere may have caused the aridity in the Jiangnan Basin (Guo et al., 2008; Quan et al., 2014), which is consistent with the occurrence of evaporites at the top and bottom of SKD1 borehole (Fig. 3A-B, E-F). Aluminum (Al) is principally derived from aluminosilicate clay minerals; titanium (Ti) is mainly associated with heavy minerals such as ilmenite, rutile, and titanite (Rimmer et al., 2004; Tribouillard et al., 2006). Both of them are generally immobile during diagenesis and burial, often considered from detrital input (Tribouillard et al., 1994). In our data, both Al₂O₃ and TiO₂ values reach peak values in the PETM, indicating enhanced terrigenous flux (Fig. 4f and g), which is consistent with the high content of clastic minerals (Fig. S1). Strontium (Sr) is more mobile and leachable than rubidium (Rb), and the Rb/Sr ratio has a positive correlation with chemical weathering in clastic rocks (Dasch, 1969). Rb/Sr also shows peak values in the PETM, indicating stronger chemical weathering intensity.

Sr in seawater is generally much higher than that in freshwater, whereas barium (Ba) does not display a significant difference between seawater and freshwater (<10 times) (Pyle et al., 2017; Wei and Algeo, 2020). Together, both Sr content and the Sr/Ba ratio in sediments show strong correlations with salinity (Wei and Algeo, 2020). At the same time, the relatively low Sr/Ba and Mg/Ca ratios we observe in the PETM interval suggest a decrease in salinity relative to the strata above and

below (Fig. 4j and k). As high temperature and more precipitation will enhance the chemical and physical weathering, and lower the salinity of the lake water (Ma et al., 2019), the above proxies suggest a wetter climate during the PETM. This agrees well with previous evaporite minerals and palynology records which reveal that the PETM was likely characterized by an extremely warm and humid climate with enhanced precipitation in the Jiangnan Basin (Teng et al., 2021; Xie et al., 2022). When the termination of the PETM, Al₂O₃ and TiO₂ and Rb/Sr values decrease, while Sr/Ba and Mg/Ca ratios increase, indicating an increase in salinity and relatively weakened chemical and physical weathering. We also note that the Rb/Sr data show additional wet/dry cycles that tie with alternately deposited mudstones and siltstones during the wet PETM period (Fig. 4e), probably related to the orbital forcing of hydroclimate fluctuations (Zhang et al., 2024).

U and Mo are depleted in sediments under oxic conditions but tend to be enriched under anoxic conditions (Algeo and Maynard, 2004; Tribouillard et al., 2006). In our data, during the PETM, all these redox proxies have relatively low values, suggesting an oxic environment. Besides, the purple-red siltstones with cross-bedded observed in the PETM interval also provide evidence of oxic conditions, since the oxidation of iron oxide to hematite will redden sediments (McBride, 1974). On the contrary, relatively high U_{EF} and Mo_{EF} values in the pre- and post-PETM intervals suggest stratified water columns with likely anoxic bottom water (Fig. 4h and j).

The chemical behavior of Ni and P under different redox conditions has been summarized in detail by Algeo and Maynard (2004) and Tribouillard et al. (2006). Ni is mainly transported to the sediments with organometallic complexes. When organic matter decays, these elements will be released and can be trapped within pyrite. Therefore, Ni abundance is considered as a marker of organic matter flux at least in part related to productivity (Tribouillard et al., 2006). Phosphorus serves as a vital nutrient for organismal growth and plays an important role in biological processes (Redfield, 1958). It is often regarded as an effective productivity indicator (Brumsack, 2006). To eliminate the influence of detrital provenance, the ratios of Ni/Al and P/Al were employed to assess paleoproductivity conditions (Algeo and Maynard, 2004; Algeo et al., 2011). During the PETM, both Ni/Al and P/Al exhibited low values consistent with the trend of TOC, indicating relatively low productivity. Conversely, elevated salinity could favor the proliferation of heterotrophic bacteria and halophilic archaea (Grice et al., 1998), which may likely make significant contributions to organic matter production in the pre- and post-PETM intervals, resulting relatively high productivity (Fig. 4l and m).

5.2. Interpretation of the organic carbon isotope

Previous study shows that the carbonate minerals in SKD1 borehole are primarily of authigenic origin and the diagenetic influence is negligible (Teng et al., 2021). Since the XGZ Formation has not been deeply buried, the burial temperature was not so high (>300 °C, (Meyers, 1994, 1997)) as to alter the carbon isotopic composition of the organic matter (Chen et al., 2023; Teng et al., 2024). In addition, both TOC and δ¹³C_{TOC} in the SKD1 core vary without obvious stratigraphic

Table 1
Ranges and averages of the geochemical data in the SKD1 borehole.

Interval		TOC (%)	Al ₂ O ₃ (%)	TiO ₂ (%)	U _{EF}	Mo _{EF}	Sr/Ba	Mg/Ca	Ni/Al (10 ⁻⁴)	P/Al (10 ⁻⁴)	Rb/Sr
Post-PETM	Minimum	0.4	0.1	0.1	5	1	1	0.2	4.4	8.01	0.01
	Maximum	6.9	11.6	0.5	47	189	34	2.2	9.8	53.21	0.15
	Average	2.3	5.2	0.3	18	53	17	0.5	6.7	21.91	0.05
PETM	Minimum	0.1	0.2	0.3	0	0	1	0.7	0.2	5.37	0.01
	Maximum	3.4	16	0.7	23	38	15	0.3	9.2	29.37	64
	Average	0.5	11.9	0.5	5	5	3	0.3	5.0	9.53	4.3
Pre-PETM	Minimum	0.1	0.9	0.1	1	3	13	0.1	1.4	7.43	0.01
	Maximum	2.7	19	0.7	21	207	101	6.6	19.7	21.37	0.9
	Average	1.4	8.2	0.5	91	59	55	0.9	8.4	13.38	0.14

trends (Fig. 4c and d), and no significant correlation between TOC and $\delta^{13}\text{C}_{\text{TOC}}$ is observed in the pre- and PETM intervals ($R^2 < 0.02$) (Fig. 5A), suggesting that the $\delta^{13}\text{C}_{\text{TOC}}$ is not influenced by organic carbon preservation in these intervals (Domingo et al., 2009). Thus, the effect of diagenesis on $\delta^{13}\text{C}_{\text{TOC}}$ can be excluded. The post-PETM sediments were deposited under high salinity and anoxic conditions, which were conducive to the development of sulfate-reducing bacteria (SRB) (Orphan et al., 2001). Their metabolic processes could cause the fractionation of organic carbon isotope, with a tendency to utilize lighter carbon isotope (e.g., ^{12}C) while retaining more heavier carbon isotope (e.g., ^{13}C) in the residual organic matter (Londry and Des Marais, 2003), which might lead to the high negative correlation between TOC and $\delta^{13}\text{C}_{\text{TOC}}$ in the post-PETM stage (Fig. 5A).

The $\delta^{13}\text{C}_{\text{TOC}}$ record shows a general similar trend with $\delta^{13}\text{C}_{\text{carb}}$ record. A clear CIE with a magnitude of around 4.3‰ occurs at a depth interval of 1376–1316 m, which represents a perturbation to the isotopic compositions of the exogenic carbon pool during the PETM (Dickens et al., 1997; Sluijs and Dickens, 2012; Chen et al., 2014). We also notice that there are differences between the $\delta^{13}\text{C}_{\text{carb}}$ and $\delta^{13}\text{C}_{\text{TOC}}$ records (Fig. 4a and c), with $\delta^{13}\text{C}_{\text{carb}}$ curve showing a long decreasing trend during the PETM, while $\delta^{13}\text{C}_{\text{TOC}}$ showing an increasing trend. This might indicate that they might not derive from the same carbon pool, and corroborate a minor impact of lake-derived organic matter, which should have a strong signature of the $\delta^{13}\text{C}$ of lake dissolved inorganic carbon (DIC). Thus, the organic carbon is mainly derived from terrestrial plants. The $\delta^{13}\text{C}_{\text{TOC}}$ values of the well SKD1 (−31.0‰ to −21.0‰) are compatible with C_3 plants (−34‰ to −23‰) (O’Leary, 1988).

5.3. Organic matter accumulation during the PETM and post-PETM

Organic matter accumulation is ultimately a balance of production and preservation, and organic matter concentrations in sediments and rocks are strongly dependent on redox conditions, primary productivity, and sediment accumulation rates (SAR) (Demaison and Moore, 1980; Tyson, 2001). Lake basins are highly sensitive to climate, and regional climate conditions can alter the depositional system and further

influence organic matter production and preservation (Carroll and Bohacs, 1999; Aswasereelert et al., 2013).

During the PETM, the relatively warming and humid climate state was associated with elevated mean annual precipitation, leading to the growth of the subtropical forest ecosystem in the surrounding hinterland to the Jiangnan Basin (Xie et al., 2022). In concert with increased runoff, this would lead to more land-derived organic matter transported into the lake, potentially increasing TOC in sediments. As the majority of organic matter during the PETM period was derived from terrestrial plants, the influence of productivity on the organic matter appears to be minimal. Enhanced rainfall has promoted lake ventilation, bringing in ample oxygen and disrupting previous anoxic conditions. The prevailing oxic environment we infer for the basin during the PETM would expedite the rate of organic matter decomposition, thus potentially resulting in reduced organic matter accumulation (Meyers, 1994; Kirschbaum, 1995) (Fig. 4d). At the same time, due to the sparse vegetation and exposed ground surface in a relatively arid pre-PETM interval, higher precipitation in the PETM could increase the soil surface erosion and cause higher terrigenous fluxes and SAR, which would serve to dilute organic matter concentration, potentially leading to reduced TOC in the sediments. Taken together, we infer that for our SKD1 record, the relatively low TOC in the PETM can be explained by both this dilution effect and the likely elevated rates of oxic bacterial organic matter degradation that would have accompanied warming. As a result, the overall preservation potential of the exported organic matter was low, hence explaining the low TOC content (avg. 0.5%) of the PETM relative to the pre- and post-PETM intervals (Fig. 6A).

In the post-PETM interval, the relatively arid climate led to increased lake salinity, which significantly effect biological processes. Under intermediate salinity conditions (10–20 ppt), sufficient nutrients strengthen phytoplankton nitrogen uptake potential and increase the abundance of bacteria associated with nitrification, thereby effectively increasing primary productivity (Kumar et al., 2018; Wang et al., 2018). Additionally, evidence from modern salt lakes suggests that certain heterotrophic bacteria and halophilic archaea can survive by effectively mitigating the adverse effects of high osmotic pressure (Strahl and Greie,

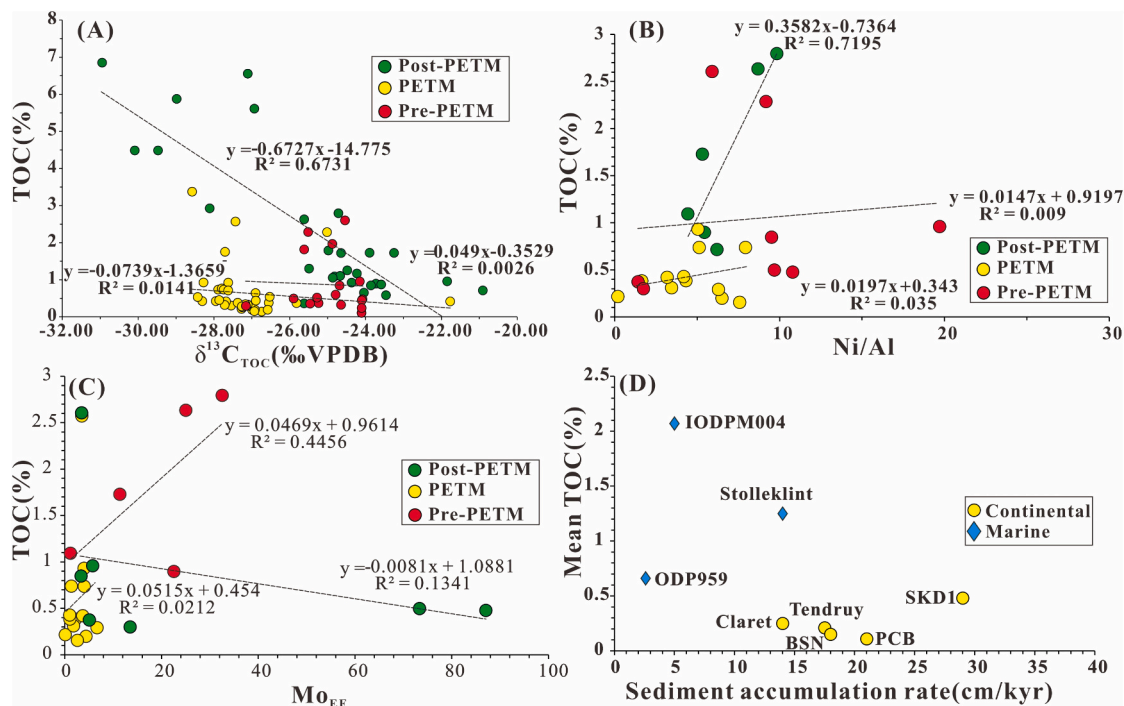


Fig. 5. Cross-plots of (A) $\delta^{13}\text{C}_{\text{TOC}}$ and TOC, (B) Ni/Al and TOC, (C) Mo_{EF} and TOC, (D) Sediment accumulation rate and mean TOC from different global records during the PETM, Ocean Drilling Program (ODP) 959 (Frieling et al., 2019), Integrated Ocean Drilling Program (IODP) M004 (Sluijs et al., 2008), Stolleklint (Stokke et al., 2020), PCB: Polecat Bench, BSN: Basin Substation (Denis et al., 2021), Claret and Tendrury sections (Domingo et al., 2009).

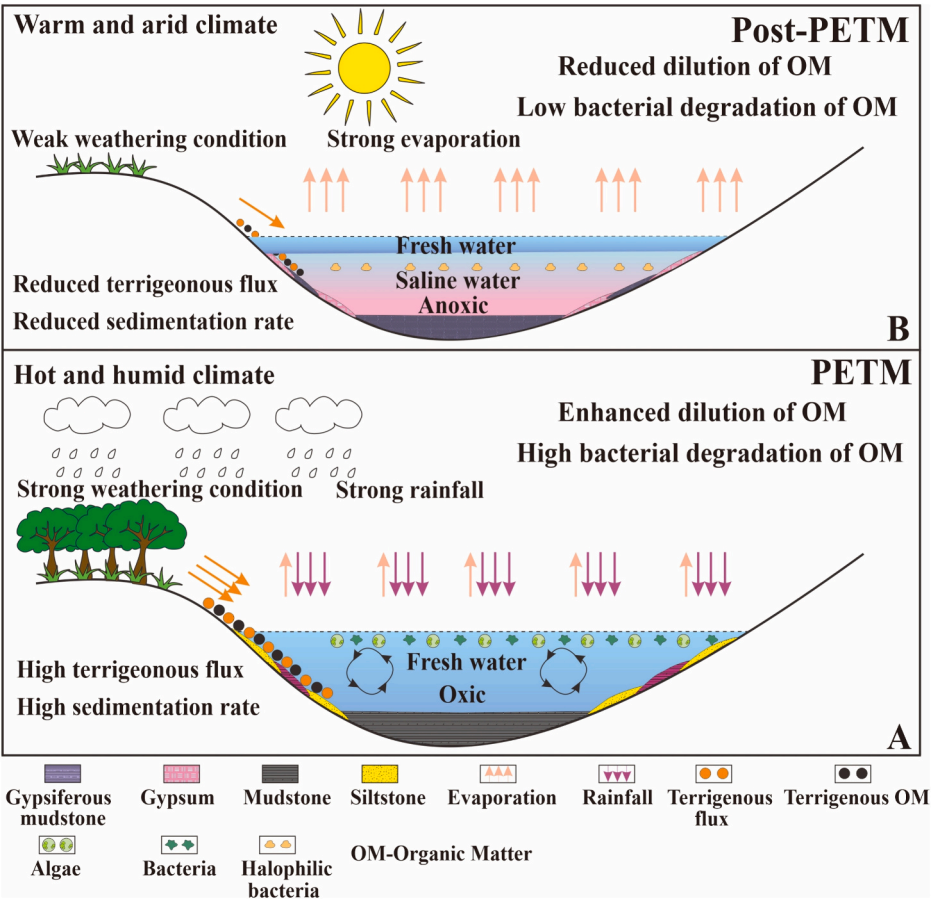


Fig. 6. Simplified organic matter enrichment models of the PETM and Post-PETM in the SKD1 borehole.

2008), thereby may significantly increasing productivity (Kelts, 1988; Deng et al., 2010; Vahed et al., 2011). These organisms may contribute to a portion of the organic matter, as indicated by the positive correlation between TOC and Ni/Al in the post-PETM interval (Fig. 5B). At the same time, the arid climate during this interval could cause higher salinity of the lake water, which would have promoted chemical and redox stratification of the lake (Eugster, 1980), and thus slowed the degradation of organic matter and increased preservation potential. This is consistent with the positive correlation between TOC and MO_{EF} (Fig. 5C). Relative to the PETM interval, the lower sediment accumulation rate of the post-PETM interval would also limit terrigenous dilution, and thus led to enhanced TOC preservation in the sediments

(Tyson, 2001). Together, these factors can explain the relatively elevated TOC observed in the post-PETM interval of the SKD1 borehole (avg. 2.3%) (Fig. 6B).

5.4. Comparison of marine and continental records of organic carbon accumulation during the PETM

Compared with marine records, TOC values of SKD1 borehole in Jiangnan Basin are lower and show no obvious trend of increase during the PETM (Fig. 5D). The above discussion emphasizes the respective roles of terrigenous dilution and redox in controlling TOC in the Jiangnan Basin during the PETM. The oxic environment we infer in the SKD1

Table. 2
Comparison of TOC records from different global sections across the PETM.

Section/ Well	Coordinate	Facies	Interval				T-test	P-value
			Pre-PETM	PETM		Post-PETM		
			Average TOC (%)	ESAR (cm/kyr)	Average TOC (%)	Average TOC (%)		
Claret-Spain	44°09'N,0°50' W	Mega-fan	0.47	14	0.25	0.72	−5.59	<0.01
Tendruy-Spain	44°10'N,0°49' W		0.16	17.5	0.21	0.61	−3.80	<0.01
Polecat	44°46'N,108°53'W		0.18	21	0.11	0.17	−1.78	<0.08
Basin	44°25'N,108°6'W	River system	0.54	18	0.15	0.27	−1.56	<0.13
Substation-USA	30°06'N,111°38'E	lake	1.42	29	0.48	2.25	−6.98	<0.01
SKD1-China	56°50'N, 8°59'E			14	1.25	0.71	4.07	<0.01
Stolleklint-Denmark	3°37'N, 2°44'W		0.32	2.6	0.66	0.33	7.58	<0.01
ODP959	87°52'N,136°11'E	Deep marine	2.26	5	2.07	1.34		
IODPM004		Shallow marine						

Notes: ESAR: Estimated sediment accumulation rates; T-test between PETM and post-PETM; Clart and Tendruy from (Domingo et al., 2009); Basin Substation and Plecat Bench from (Denis et al., 2021); Stolleklint from (Stokke et al., 2020); ODP959 from (Frieling et al., 2019); IODPM004 from (Sluijs et al., 2008).

record was unfavorable for preservation of the organic matter, and enhanced terrestrial flux might also have caused dilution of the organic matter. To test if the low TOC and the low organic matter accumulation during the PETM was a spatially widespread phenomenon in terrestrial basins, we compare our results with other TOC records from four terrestrial sites (Table 2) (Figs. 1A and 7).

The relatively low TOC during the PETM that we observe in the Jiangnan Basin is also apparent at other terrestrial sites in Spain (Claret Conglomerate; Domingo et al., 2009), Bighorn Basin (Magioncalda et al., 2004) and Piceance Basin (Denis et al., 2021) in the USA (Table 2) (Figs. 1A, and 7). These continental TOC records from diverse settings (lake, river, and megafan depositional environments, Table 2) suggest that relatively low TOC during the PETM in continental environments might be a widespread phenomenon, at least in subtropical to mid-latitude regions. An independent *t*-test shows that TOC is significantly higher in the post-PETM intervals of the studied locations (Table 2). Our analysis shows that all the TOC records in terrestrial sites are generally low compared to that in the marine sites (Fig. 5D). For marine settings, sea level rise, enhanced productivity, anoxic water conditions, and relatively low SAR together improved productivity and preservation conditions (Sluijs et al., 2008). As a result, elevated organic carbon burial is believed to have significantly contributed to the sequestration of injected carbon at the PETM (Sluijs et al., 2008; Soliman et al., 2011). However, in continental environments, the scenario may be entirely different.

Work on the Bighorn and Piceance basins has previously suggested that the reduction in TOC in PETM samples at these sites was likely the result of decreased preservation (Denis et al., 2021), though decreased organic carbon production may have contributed as well (McInerney and Wing, 2011). Denis et al. (2021) proposed that the increase in oxidation/decay rate of organic matter during the PETM might have contributed to unfavorable conditions for organic matter preservation and, consequently, to the carbon burial efficiency during the PETM.

Higher SAR has complex effects on organic matter preservation. On

the one hand, it can let inorganic minerals rapidly deposit in sediments and thus cause a dilution effect (Stein, 1990; Tyson, 2001). On the other hand, under oxic environment, high SAR will reduce the exposure time for the oxidation of organic matter at the sediment-water interface (Tyson, 2001; Kemp et al., 2022). The estimated sediment accumulation rates (ESAR) of the SKD1 borehole and the rest sections/wells were calculated by dividing thickness by time (Table 2), assuming the duration of PETM is 200 ka (Westerhold et al., 2018). In comparison to marine sites, the observed lower TOC content in terrestrial records may be attributed in part to the dilution effect induced by higher SAR (Fig. 5D). Overall, organic matter accumulation during the PETM in a terrestrial setting might be mainly controlled by the preservation condition and SAR, which were linked to climate and hydrology.

6. Conclusions

Our new multiproxy data from the SKD1 borehole of the Jiangnan Basin provides new information on changes in hydrology and lake water chemistry in this saline lacustrine basin across the PETM. Analysis of TOC and multiple geochemical proxies suggest that compared with marine records, there is no obvious increase of TOC in the Jiangnan Basin during the PETM, and this was mainly caused by the poor preservation condition and high SAR, which were closely linked with hydrology/climate. Specifically, high temperature would expedite organic matter decomposition during the PETM; enhanced precipitation could, on the one hand, cause a prevailing oxic environment due to bringing in ample oxygen and disrupting previous water column stratification caused by high salinity; on the other hand, increasing terrigenous flux would also dilute organic matter, causing a lowering of TOC. In contrast, the increased salinity, due to the arid condition after the PETM, could promote stratification of the water column and anoxic environment, which effectively slowed the degradation of organic matter. And the lower SAR could weaken the terrigenous dilution effects, leading to relatively high TOC. The poor preservation condition of the organic

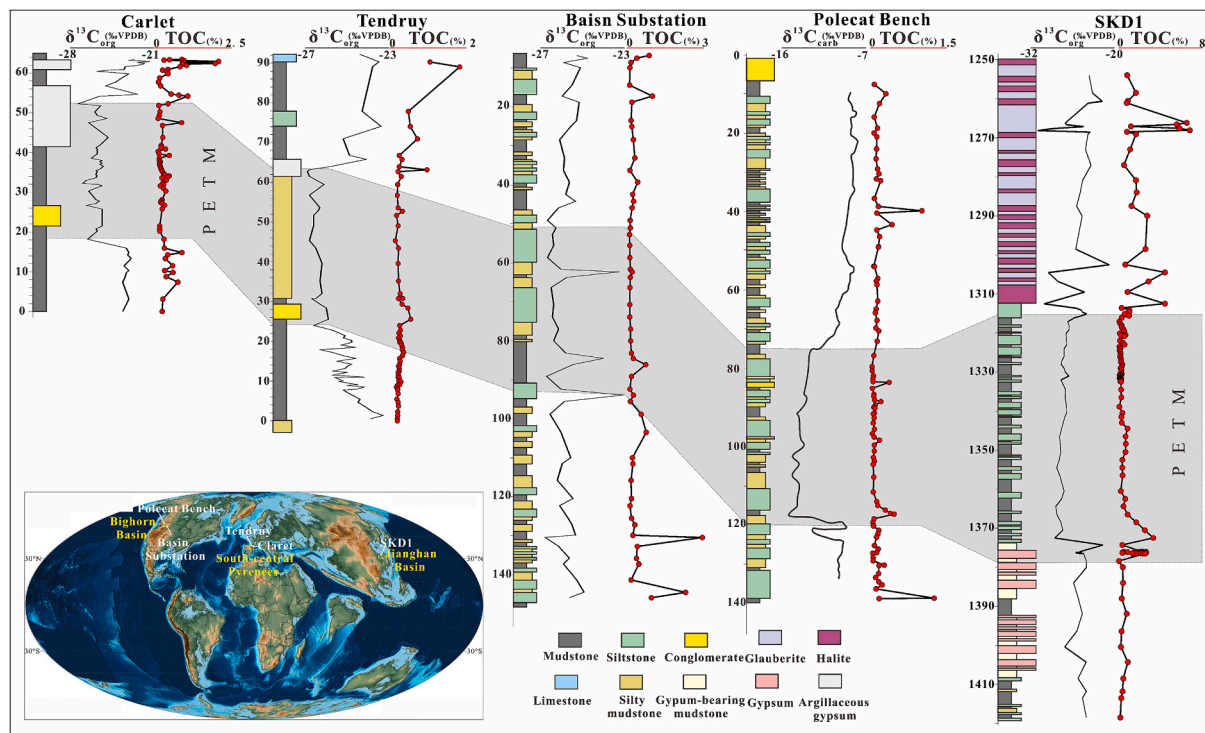


Fig. 7. Continental $\delta^{13}\text{C}_{\text{TOC}}$ and TOC curves of Claret and Tendry sections (South-central Pyrenees, Lleida, Spain; Domingo et al., 2009), Basin Substation (Denis et al., 2021), SKD1 borehole, and $\delta^{13}\text{C}_{\text{carb}}$ and TOC record from Polecat Bench (Bighorn Basin, Wyoming, USA; Bowen et al., 2015). Colors are only used to distinguish lithology.

matter and higher SAR might also have been the primary factors for the low TOC in PETM terrestrial sections at other subtropical and mid-latitude locations. Our records imply that in contrast to marine settings, terrestrial settings may exhibit lower efficiency in sequestering excess CO₂ from the atmosphere through organic carbon burial during the PETM.

CRediT authorship contribution statement

Xiaojie Fan: Writing – original draft, Methodology, Conceptualization, Validation. **Chunlian Wang:** Writing – original draft, Resources, Funding acquisition, Conceptualization. **Xiaohua Teng:** Writing – review & editing, Supervision, Resources, Funding acquisition, Data curation, Conceptualization. **David B. Kemp:** Writing – review & editing, Validation, Methodology, Funding acquisition. **Yangbo Lu:** Visualization, Validation, Investigation, Data curation. **Kai Yan:** Visualization, Validation, Software, Data curation. **Wei Wei:** Software, Methodology, Formal analysis. **Jingyu Zhang:** Writing – review & editing, Supervision, Resources, Methodology, Funding acquisition, Conceptualization.

Declaration of competing interest

The authors declare that they have no known competing financial interests or personal relationships that could have appeared to influence the work reported in this paper.

Data availability

Data will be made available on request.

Acknowledgements

This work was supported by the National Natural Science Foundation of China (41907262, 42304082, U20A2092, 42002106), China Scholarship Council (CSC202206410111), the China Postdoctoral Science Foundation (No. 2022M721461) and National Key R&D Program of China Program of China (No. 2023YFF0804000).

Appendix A. Supplementary data

Supplementary data to this article can be found online at <https://doi.org/10.1016/j.palaeo.2024.112283>.

References

- Algeo, T.J., Maynard, J.B., 2004. Trace-element behavior and redox facies in core shales of Upper Pennsylvanian Kansas-type cyclothems. *Chem. Geol. Geochem. Organic-Rich Shales: New Perspectives* 206, 289–318. <https://doi.org/10.1016/j.chemgeo.2003.12.009>.
- Algeo, T.J., Kuwahara, K., Sano, H., Bates, S., Lyons, T., Elswick, E., Hinnov, L., Ellwood, B., Moser, J., Maynard, J.B., 2011. Spatial variation in sediment fluxes, redox conditions, and productivity in the Permian–Triassic Panthalassic Ocean. *Palaeogeogr. Palaeoclimatol. Palaeoecol.* 308, 65–83.
- Aswasereelert, W., Meyers, S.R., Carroll, A.R., Peters, S.E., Smith, M.E., Feigl, K.L., 2013. Basin-scale cyclostratigraphy of the Green River Formation, Wyoming. *GSA Bull.* 125, 216–228. <https://doi.org/10.1130/B30541.1>.
- Berner, R.A., 2003. The long-term carbon cycle, fossil fuels and atmospheric composition. *Nature* 426, 323–326. <https://doi.org/10.1038/nature02131>.
- Bowen, G.J., Maibauer, B.J., Kraus, M.J., Röhl, U., Westerhold, T., Steimke, A., Gingerich, P.D., Wing, S.L., Clyde, W.C., 2015. Two massive, rapid releases of carbon during the onset of the Palaeocene-Eocene thermal maximum. *Nat. Geosci.* 8, 44–47. <https://doi.org/10.1038/ngeo2316>.
- Brumsack, H.-J., 2006. The trace metal content of recent organic carbon-rich sediments: implications for cretaceous black shale formation. *Palaeogeogr. Palaeoclimatol. Palaeoecol.* 232, 344–361.
- Carroll, A.R., Bohacs, K.M., 1999. Stratigraphic classification of ancient lakes: Balancing tectonic and climatic controls. *Geology* 27, 99–102. [https://doi.org/10.1130/0091-7613\(1999\)027<0099:SCOALB>2.3.CO;2](https://doi.org/10.1130/0091-7613(1999)027<0099:SCOALB>2.3.CO;2).
- Chen, Z., Wang, X., Hu, J., Yang, S., Zhu, M., Dong, X., Tang, Z., Peng, P., Ding, Z., 2014. Structure of the carbon isotope excursion in a high-resolution lacustrine Paleocene–Eocene Thermal Maximum record from central China. *Earth Planet. Sci. Lett.* 408, 331–340. <https://doi.org/10.1016/j.epsl.2014.10.027>.
- Chen, Z., Ding, Z., Sun, J., Yang, S., Ni, X., Wang, X., Wang, Y., Zhang, J., He, W., 2023. Freshwater ecosystem collapse and mass mortalities at the Paleocene-Eocene thermal maximum. *Glob. Planet. Chang.* 227, 104175. <https://doi.org/10.1016/j.gloplacha.2023.104175>.
- Dasch, E.J., 1969. Strontium isotopes in weathering profiles, deep-sea sediments, and sedimentary rocks. *Geochim. Cosmochim. Acta* 33, 1521–1552. [https://doi.org/10.1016/0016-7037\(69\)90153-7](https://doi.org/10.1016/0016-7037(69)90153-7).
- Demaison, G.J., Moore, G.T., 1980. Anoxic environments and oil source bed genesis. *Org. Geochem.* 2, 9–31. [https://doi.org/10.1016/0146-6380\(80\)90017-0](https://doi.org/10.1016/0146-6380(80)90017-0).
- Deng, S., Dong, H., Lv, G., Jiang, H., Yu, B., Bishop, M.E., 2010. Microbial dolomite precipitation using sulfate reducing and halophilic bacteria: results from Qinghai Lake, Tibetan Plateau, NW China. *Chem. Geol.* 278, 151–159. <https://doi.org/10.1016/j.chemgeo.2010.09.008>.
- Denis, E.H., Maibauer, B.J., Bowen, G.J., Jardine, P.E., Harrington, G.J., Baczynski, A.A., McInerney, F.A., Collinson, M.E., Belcher, C.M., Wing, S.L., Freeman, K.H., 2021. Decreased soil carbon in a warming world: Degraded pyrogenic carbon during the Paleocene-Eocene thermal Maximum, Bighorn Basin Wyoming. *Earth Planet. Sci. Lett.* 566, 116970. <https://doi.org/10.1016/j.epsl.2021.116970>.
- Dickens, G.R., O'Neil, J.R., Rea, D.K., Owen, R.M., 1995. Dissociation of oceanic methane hydrate as a cause of the carbon isotope excursion at the end of the Paleocene. *Paleoceanography* 10, 965–971. <https://doi.org/10.1029/95PA02087>.
- Dickens, G.R., Castillo, M.M., Walker, J.C.G., 1997. A blast of gas in the latest Paleocene: Simulating first-order effects of massive dissociation of oceanic methane hydrate. *Geol.* 25, 259. [https://doi.org/10.1130/0091-7613\(1997\)025<0259:ABOGIT>2.3.CO;2](https://doi.org/10.1130/0091-7613(1997)025<0259:ABOGIT>2.3.CO;2).
- Domingo, L., López-Martínez, N., Leng, M.J., Grimes, S.T., 2009. The Paleocene–Eocene Thermal Maximum record in the organic matter of the Claret and Tendrúy continental sections (South-central Pyrenees, Lleida, Spain). *Earth Planet. Sci. Lett.* 281, 226–237. <https://doi.org/10.1016/j.epsl.2009.02.025>.
- Drake, T.W., Raymond, P.A., Spencer, R.G.M., 2018. Terrestrial carbon inputs to inland waters: a current synthesis of estimates and uncertainty. *Limnol. Oceanogr. Lett.* 3, 132–142. <https://doi.org/10.1002/lol2.10055>.
- Eugster, H.P., 1980. Geochemistry of evaporitic lacustrine deposits. *Annu. Rev. Earth Planet. Sci.* 8, 35–63.
- Frieling, J., Peterse, F., Lunt, D.J., Bohaty, S.M., Sinninghe Damsté, J.S., Reichert, G.-J., Sluijs, A., 2019. Widespread Warming before and Elevated Barium Burial during the Paleocene-Eocene thermal Maximum: evidence for methane Hydrate Release? *Paleoceanogr. Palaeoclimatol.* 34, 546–566. <https://doi.org/10.1029/2018PA003425>.
- Gradstein, F.M., Ogg, J.G., Schmitz, M.D., Ogg, G.M., 2020. *Geologic time scale 2020*. Elsevier.
- Grice, K., Schouten, S., Peters, K.E., Sinninghe Damsté, J.S., 1998. Molecular isotopic characterisation of hydrocarbon biomarkers in Palaeocene–Eocene evaporitic, lacustrine source rocks from the Jiangnan Basin, China. *Org. Geochem.* 29, 1745–1764. [https://doi.org/10.1016/S0146-6380\(98\)00075-8](https://doi.org/10.1016/S0146-6380(98)00075-8).
- Guo, Z.T., Sun, B., Zhang, Z.S., Peng, S.Z., Xiao, G.Q., Ge, J.Y., Hao, Q.Z., Qiao, Y.S., Liang, M.Y., Liu, J.F., Yin, Q.Z., Wei, J.J., 2008. A major reorganization of Asian climate by the early Miocene. *Clim. Past* 4, 153–174. <https://doi.org/10.5194/cp-4-153-2008>.
- Hu, S., Kohn, B.P., Raza, A., Wang, J., Gleadow, A.J.W., 2006. Cretaceous and Cenozoic cooling history across the ultrahigh pressure Tongbai–Dabie belt, central China, from apatite fission-track thermochronology. *Tectonophysics* 420, 409–429. <https://doi.org/10.1016/j.tecto.2006.03.027>.
- Huang, C., Hinnov, L., 2014. Evolution of an Eocene-Oligocene saline lake depositional system and its controlling factors, Jiangnan Basin, China. *J. Earth Sci.* 25, 959–976. <https://doi.org/10.1007/s12583-014-0499-2>.
- Huang, C., Hinnov, L., 2019. Astronomically forced climate evolution in a saline lake record of the middle Eocene to Oligocene, Jiangnan Basin, China. *Earth Planet. Sci. Lett.* 528, 115846. <https://doi.org/10.1016/j.epsl.2019.115846>.
- Jenkyns, H.C., 2010. Geochemistry of oceanic anoxic events. *Geochem. Geophys. Geosyst.* 11. <https://doi.org/10.1029/2009GC002788>.
- John, C.M., Bohaty, S.M., Zachos, J.C., Sluijs, A., Gibbs, S., Brinkhuis, H., Bralower, T.J., 2008. North American continental margin records of the Paleocene-Eocene thermal maximum: Implications for global carbon and hydrological cycling. *Paleoceanography* 23. <https://doi.org/10.1029/2007PA001465>.
- Jones, D.T., Manners, H.R., Hoggett, M., Turner, S.K., Westerhold, T., Leng, M.J., Pancost, R.D., Ridgwell, A., Alegret, L., Duller, R., Grimes, S.T., 2018. Dynamics of sediment flux to a bathyal continental margin section through the Paleocene–Eocene Thermal Maximum. *Clim. Past* 14, 1035–1049. <https://doi.org/10.5194/cp-14-1035-2018>.
- Kaya, M.Y., Dupont-Nivet, G., Frieling, J., Fioroni, C., Rohrmann, A., Altner, S.O., Vardar, E., Tanyaş, H., Mamtimin, M., Zhaojie, G., 2022. The Eurasian epicontinental sea was an important carbon sink during the Palaeocene-Eocene thermal maximum. *Commun. Earth Environ.* 3, 1–10. <https://doi.org/10.1038/s43247-022-00451-4>.
- Kelts, K., 1988. Environments of deposition of lacustrine petroleum source rocks: an introduction. *Geol. Soc. Lond. Spec. Publ.* 40, 3–26.
- Kemp, D.B., Suan, G., Fantasia, A., Jin, S., Chen, W., 2022. Global organic carbon burial during the Toarcian oceanic anoxic event: patterns and controls. *Earth-Sci. Rev.* 231, 104086. <https://doi.org/10.1016/j.earscirev.2022.104086>.
- Kennett, J.P., Stott, L.D., 1991. Abrupt deep-sea warming, palaeoceanographic changes and benthic extinctions at the end of the Palaeocene. *Nature* 353, 225–229. <https://doi.org/10.1038/353225a0>.

- Kirschbaum, M.U.F., 1995. The temperature dependence of soil organic matter decomposition, and the effect of global warming on soil organic C storage. *Soil Biol. Biochem.* 27, 753–760. [https://doi.org/10.1016/0038-0717\(94\)00242-S](https://doi.org/10.1016/0038-0717(94)00242-S).
- Kong, X., Jiang, Z., Wu, S., Ge, T., 2024. Stepwise astronomical tuning of obliquity-driven evaporite cycles in an Eocene salt lake (Jiangnan Basin, Hubei Province, China): Implications for middle Eocene East Asian monsoon-like climate evolution. *Geol. Soc. Am. Bull.* 136.
- Kumar, S., Bhavya, P.S., Ramesh, R., Gupta, G.V.M., Chiriboga, F., Singh, A., Karunasagar, I., Rai, A., Rehnstam-Holm, A.-S., Edler, L., Godhe, A., 2018. Nitrogen uptake potential under different temperature-salinity conditions: Implications for nitrogen cycling under climate change scenarios. *Mar. Environ. Res.* 141, 196–204. <https://doi.org/10.1016/j.marenvres.2018.09.001>.
- Laurin, J., Meyers, S.R., Uličný, D., Jarvis, I., Sageman, B.B., 2015. Axial obliquity control on the greenhouse carbon budget through middle- to high-latitude reservoirs. *Paleoceanography* 30, 133–149. <https://doi.org/10.1002/2014PA002736>.
- Londry, K.L., Des Marais, D.J., 2003. Stable Carbon Isotope Fractionation by Sulfate-reducing Bacteria. *Appl. Environ. Microbiol.* 69, 2942–2949. <https://doi.org/10.1128/AEM.69.5.2942-2949.2003>.
- Luo, X., Wang, P., Luo, C., Lv, M., Li, S., Wei, X., 2023. Paleocene-Eocene carbon isotope excursion recorded in the western Jiangnan Basin, China (no. EGU23-10485). Presented at the EGU23. Copernicus Meetings. <https://doi.org/10.5194/egusphere-egu23-10485>.
- Ma, Y., Fan, M., Li, M., Ogg, J.G., Zhang, C., Feng, J., Zhou, C., Liu, X., Lu, Y., Liu, H., Eldrett, J.S., Ma, C., 2023. East Asian lake hydrology modulated by global sea-level variations in the Eocene warmhouse. *Earth and Planet. Sci. Lett.* 602, 117925.
- Ma, Y., Fan, M., Lu, Y., Liu, H., Zhang, S., Liu, X., 2019. Stable isotope record of middle Eocene summer monsoon and its instability in eastern China. *Global and Planetary Change* 175, 103–112.
- Magioncalda, R., Dupuis, C., Smith, T., Steurbaut, E., Gingerich, P.D., 2004. Paleocene-Eocene carbon isotope excursion in organic carbon and pedogenic carbonate: Direct comparison in a continental stratigraphic section. *Geology* 32, 553–556. <https://doi.org/10.1130/G20476.1>.
- McBride, E.F., 1974. Significance of color in red, green, purple, olive, brown, and gray beds of Difunta Group, northeastern Mexico. *J. Sediment. Res.* 44, 760–773. <https://doi.org/10.1306/212F6B9A-2B24-11D7-8648000102C1865D>.
- McInerney, F.A., Wing, S.L., 2011. The Paleocene-Eocene thermal Maximum: a Perturbation of Carbon Cycle, climate, and Biosphere with Implications for the Future. *Annu. Rev. Earth Planet. Sci.* 39, 489–516. <https://doi.org/10.1146/annurev-earth-040610-133431>.
- McLennan, S.M., 2001. Relationships between the trace element composition of sedimentary rocks and upper continental crust. *Geochim. Geophys. Geosyst.* 2. <https://doi.org/10.1029/2000GC000109>.
- Mendonça, R., Müller, R.A., Clow, D., Verpoorter, C., Raymond, P., Tranvik, L.J., Sobek, S., 2017. Organic carbon burial in global lakes and reservoirs. *Nat. Commun.* 8, 1694. <https://doi.org/10.1038/s41467-017-01789-6>.
- Meyers, P.A., 1994. Preservation of elemental and isotopic source identification of sedimentary organic matter. *Chem. Geol.* 114, 289–302. [https://doi.org/10.1016/0009-2541\(94\)90059-0](https://doi.org/10.1016/0009-2541(94)90059-0).
- Meyers, P.A., 1997. Organic geochemical proxies of paleoceanographic, paleolimnologic and paleoclimatic processes. *Org. Geochem.* 27, 213–250.
- O'Leary, M.H., 1988. Carbon Isotopes in Photosynthesis. *BioScience* 38, 328–336. <https://doi.org/10.2307/1310735>.
- Orphan, V.J., Hinrichs, K.-U., Ussler, W., Paull, C.K., Taylor, L.T., Sylva, S.P., Hayes, J.M., Delong, E.F., 2001. Comparative Analysis of Methane-Oxidizing Archaea and Sulfate-reducing Bacteria in Anoxic Marine Sediments. *Appl. Environ. Microbiol.* 67, 1922–1934. <https://doi.org/10.1128/AEM.67.4.1922-1934.2001>.
- Papadomanolaki, N.M., Sluijs, A., Slomp, C.P., 2022. Eutrophication and Deoxygenation Forcing of marginal Marine Organic Carbon Burial during the PETM. *Paleoceanogr. Paleoclimatol.* 37, e2021PA004232. <https://doi.org/10.1029/2021PA004232>.
- Philp, R.P., Jinggui, L., Lewis, C.A., 1989. An organic geochemical investigation of crude oils from Shangannan, Jiangnan, Chaidamu and Zhungeer Basins, People's Republic of China. *Org. Geochem.* 14, 447–460. [https://doi.org/10.1016/0146-6380\(89\)90010-7](https://doi.org/10.1016/0146-6380(89)90010-7).
- Pierrehumbert, R.T., 2002. The hydrologic cycle in deep-time climate problems. *Nature* 419, 191–198. <https://doi.org/10.1038/nature01088>.
- Pyle, K.M., Hendry, K.R., Sherrell, R.M., Meredith, M.P., Venables, H., Lagerström, M., Morte-Ródenas, A., 2017. Coastal barium cycling at the West Antarctic Peninsula deep sea research part ii: topical studies in oceanography. *Adv. understanding marine system west Antarctic Peninsula* 139, 120–131. <https://doi.org/10.1016/j.dsr2.2016.11.010>.
- Quan, C., Liu, Z., Utescher, T., Jin, J., Shu, J., Li, Y., Liu, Y.-S., Christopher, 2014. Revisiting the Paleogene climate pattern of East Asia: a synthetic review. *Earth Sci. Rev.* 139, 213–230. <https://doi.org/10.1016/j.earscirev.2014.09.005>.
- Raven, M.R., Fike, D.A., Gomes, M.L., Webb, S.M., Bradley, A.S., McClelland, H.-L.O., 2018. Organic carbon burial during OAE2 driven by changes in the locus of organic matter sulfurization. *Nat. Commun.* 9, 3409. <https://doi.org/10.1038/s41467-018-05943-6>.
- Redfield, A.C., 1958. The Biological Control of Chemical Factors in the Environment. *Am. Sci.* 46, 220A–230A.
- Rimmer, S.M., Thompson, J.A., Goodnight, S.A., Robl, T.L., 2004. Multiple Controls on the Preservation of Organic Matter in Devonian–Mississippian Marine Black Shales: Geochemical and Petrographic Evidence.
- Schellart, W.P., Lister, G.S., 2005. The role of the East Asian active margin in widespread extensional and strike-slip deformation in East Asia. *J. Geol. Soc. Lond.* 162, 959–972. <https://doi.org/10.1144/0016-764904-112>.
- Scotese, C.R., 2014. Atlas of Paleogene paleogeographic maps (Mollweide projection). In: *Maps 8–15, Volume 1, the Cenozoic, PALEOMAP Atlas for ArcGIS. PALEOMAP Project, Evanston, IL.*
- Sluijs, A., Dickens, G.R., 2012. Assessing offsets between the $\delta^{13}\text{C}$ of sedimentary components and the global exogenic carbon pool across early Paleogene carbon cycle perturbations. *Global Biogeochem. Cycles* 26. <https://doi.org/10.1029/2011GB004224>.
- Sluijs, A., Röhl, U., Schouten, S., Brumsack, H.-J., Sangiorgi, F., Sinninghe Damsté, J.S., Brinkhuis, H., 2008. Arctic late Paleocene–early Eocene paleoenvironments with special emphasis on the Paleocene-Eocene thermal maximum (Lomonosov Ridge, Integrated Ocean Drilling Program Expedition 302). *Paleoceanography* 23. <https://doi.org/10.1029/2007PA001495>.
- Sluijs, A., Schouten, S., Donders, T.H., Schoon, P.L., Röhl, U., Reichert, G.-J., Sangiorgi, F., Kim, J.-H., Sinninghe Damsté, J.S., Brinkhuis, H., 2009. Warm and wet conditions in the Arctic region during Eocene thermal Maximum 2. *Nat. Geosci.* 2, 777–780. <https://doi.org/10.1038/ngeo668>.
- Soliman, M.F., Aubry, M.-P., Schmitz, B., Sherrell, R.M., 2011. Enhanced coastal paleoproductivity and nutrient supply in Upper Egypt during the Paleocene/Eocene thermal Maximum (PETM): Mineralogical and geochemical evidence. *Paleoceanogr. Paleoclimatol. Palaeoecol.* 310, 365–377. <https://doi.org/10.1016/j.paleo.2011.07.027>.
- Stein, R., 1990. Organic carbon content/sedimentation rate relationship and its paleoenvironmental significance for marine sediments. *Geo-Mar. Lett.* 10, 37–44. <https://doi.org/10.1007/BF02431020>.
- Stokke, E.W., Jones, M.T., Tierney, J.E., Svensen, H.H., Whiteside, J.H., 2020. Temperature changes across the Paleocene-Eocene thermal Maximum – a new high-resolution TEX86 temperature record from the Eastern North Sea Basin. *Earth Planet. Sci. Lett.* 544, 116388. <https://doi.org/10.1016/j.epsl.2020.116388>.
- Strahl, H., Greie, J.-C., 2008. The extremely halophilic archaeon *Halobacterium salinarum* R1 responds to potassium limitation by expression of the K⁺-transporting KdpFABC P-type ATPase and by a decrease in intracellular K⁺. *Extremophiles* 12, 741–752. <https://doi.org/10.1007/s00792-008-0177-3>.
- Teng, X., Fang, X., Kaufman, A.J., Liu, C., Wang, J., Zan, J., Yang, Y., Wang, C., Xu, H., Schulte, R.F., Piatak, N.M., 2019. Sedimentological and mineralogical records from drill core SKD1 in the Jiangnan Basin, Central China, and their implications for late Cretaceous–early Eocene climate change. *J. Asian Earth Sci.* 182, 103936. <https://doi.org/10.1016/j.jseaes.2019.103936>.
- Teng, X., Wang, C., Liu, C., Yan, K., Luo, Z., 2021. Paleocene-Eocene thermal Maximum lacustrine sediments in deep drill core SKD1 in the Jiangnan Basin: a record of enhanced precipitation in Central China. *Glob. Planet. Chang.* 205, 103620. <https://doi.org/10.1016/j.gloplacha.2021.103620>.
- Teng, X., Wang, C., Zhang, J., Yan, K., Yu, X., Zhang, D., Sluijs, A., 2024. Evidence for Poleward Migration of the Asian Monsoon during the Paleocene-Eocene Thermal Maximum. *Paleoceanography and Paleoclimatology*, Under review.
- Tribouillard, N.-P., Desprairies, A., Lallier-Vergès, E., Bertrand, P., Moureau, N., Ramdani, A., Ramanampisoa, L., 1994. Geochemical study of organic-matter rich cycles from the Kimmeridge Clay Formation of Yorkshire (UK): productivity versus anoxia. *Paleoceanogr. Palaeoclimatol. Palaeoecol.* 108, 165–181. [https://doi.org/10.1016/0031-0182\(94\)90028-0](https://doi.org/10.1016/0031-0182(94)90028-0).
- Tribouillard, N., Algeo, T.J., Lyons, T., Riboulleau, A., 2006. Trace metals as paleoredox and paleoproductivity proxies: an update. *Chem. Geol.* 232, 12–32. <https://doi.org/10.1016/j.chemgeo.2006.02.012>.
- Tripathi, A., Elderfield, H., 2005. Deep-Sea Temperature and Circulation changes at the Paleocene-Eocene thermal Maximum. *Science* 308, 1894–1898. <https://doi.org/10.1126/science.1109202>.
- Tyson, R.V., 2001. Sedimentation rate, dilution, preservation and total organic carbon: some results of a modelling study. *Org. Geochem.* 32, 333–339. [https://doi.org/10.1016/S0146-6380\(00\)00161-3](https://doi.org/10.1016/S0146-6380(00)00161-3).
- Vahed, S.Z., Forouhandeh, H., Hassanzadeh, S., Klenk, H.-P., Hejazi, M.A., Hejazi, M.S., 2011. Isolation and characterization of halophilic bacteria from Urmia Lake in Iran. *Microbiology* 80, 834–841. <https://doi.org/10.1134/S0026261711060191>.
- Walker, J.C.G., Hays, P.B., Kasting, J.F., 1981. A negative feedback mechanism for the long-term stabilization of Earth's surface temperature. *J. Geophys. Res.* 86, 9776–9782. <https://doi.org/10.1029/JC086iC10p09776>.
- Wang, H., Gilbert, J.A., Zhu, Y., Yang, X., 2018. Salinity is a key factor driving the nitrogen cycling in the mangrove sediment. *Sci. Total Environ.* 631–632, 1342–1349. <https://doi.org/10.1016/j.scitotenv.2018.03.102>.
- Wei, W., Algeo, T.J., 2020. Elemental proxies for paleosalinity analysis of ancient shales and mudrocks. *Geochim. Cosmochim. Acta* 287, 341–366. <https://doi.org/10.1016/j.gca.2019.06.034>.
- Westerhold, T., Röhl, U., Donner, B., Zachos, J.C., 2018. Global Extent of early Eocene Hyperthermal events: a New Pacific Benthic Foraminiferal Isotope Record from Shatsky rise (ODP Site 1209). *Paleoceanogr. Paleoclimatol.* 33, 626–642. <https://doi.org/10.1029/2017PA003306>.
- Westerhold, T., Marwan, N., Drury, A.J., Liebrand, D., Agnini, C., Anagnostou, E., Barnett, J.S.K., Bohaty, S.M., De Vleeschouwer, D., Florindo, F., Frederichs, T., Hodell, D.A., Holbourn, A.E., Kroon, D., Lauretano, V., Littler, K., Lourens, L.J., Lyle, M., Pälike, H., Röhl, U., Tian, J., Wilkens, R.H., Wilson, P.A., Zachos, J.C., 2020. An astronomically dated record of Earth's climate and its predictability over the last 66 million years. *Science* 369, 1383–1387. <https://doi.org/10.1126/science.aba6853>.
- Wu, L., Mei, L., Liu, Y., Luo, J., Min, C., Lu, S., Li, M., Guo, L., 2017. Multiple provenance of rift sediments in the composite basin-mountain system: Constraints from detrital zircon U-Pb geochronology and heavy minerals of the early Eocene Jiangnan Basin, Central China. *Sediment. Geol.* 349, 46–61. <https://doi.org/10.1016/j.sedgeo.2016.12.003>.

- Wu, Q., Cui, Y., Wang, Y., Jiang, S., Dong, Y., Shen, J., 2024. Biogeochemical responses to global warming during the Paleocene–Eocene Thermal Maximum in the eastern Tethys. *Palaeogeogr. Palaeoclimatol. Palaeoecol.* 636, 111969 <https://doi.org/10.1016/j.palaeo.2023.111969>.
- Xie, Y., Wu, F., Fang, X., 2022. A transient south subtropical forest ecosystem in Central China driven by rapid global warming during the Paleocene–Eocene thermal Maximum. *Gondwana Res.* 101, 192–202. <https://doi.org/10.1016/j.gr.2021.08.005>.
- Xu, L., Nan, C., Yu, H., Wang, B., Yu, F., Wang, D., 1995. Chronology of Paleogene volcanic rocks in the Jiangnan Basin. *Oil Gas Geol.* 16, 132–137 (in Chinese with English abstract).
- Yan, K., Wang, C., Liu, C., Mischke, S., Wang, J., Yu, X., 2022. Reconstruction of early Paleogene landscapes and climate in the Jiangnan Basin, Central China: evidence from evaporites and palynology. *Palaeogeogr. Palaeoclimatol. Palaeoecol.* 601, 111095 <https://doi.org/10.1016/j.palaeo.2022.111095>.
- Zachos, J.C., Dickens, G.R., Zeebe, R.E., 2008. An early Cenozoic perspective on greenhouse warming and carbon-cycle dynamics. *Nature* 451, 279–283. <https://doi.org/10.1038/nature06588>.
- Zeebe, R.E., Ridgwell, A., Zachos, J.C., 2016. Anthropogenic carbon release rate unprecedented during the past 66 million years. *Nat. Geosci.* 9, 325–329. <https://doi.org/10.1038/ngeo2681>.
- Zhang, S., Shen, H., Qu, X., Gao, Q., 1993. Tertiary in Petroliferous Regions of China (V): the Hubei–HenanAnhui Region. *Petrol. Industry Press, Beijing*, p. 296.
- Zhang, J., Wang, C., Teng, X., Kemp, D.B., Wang, Z., Yang, H., Gai, C., Zhang, Y., Zhong, Y., Jiang, X., 2024. Orbital modulation of an intensified hydrological cycle during the Paleocene–Eocene thermal Maximum. *Earth Planet. Sci. Lett.* 635, 118693.